

# Investigation of Mixed Element Hybrid Grid-Based CFD Methods for Rotorcraft Flow Analysis

Glen R. Whitehouse and Alexander H. Boschitsch  
[glen@continuum-dynamics.com](mailto:glen@continuum-dynamics.com) [alex@continuum-dynamics.com](mailto:alex@continuum-dynamics.com)  
Continuum Dynamics, Inc.  
Ewing, New Jersey, 08618, USA

Marilyn J. Smith and C. Eric Lynch  
[marilyn.smith@ae.gatech.edu](mailto:marilyn.smith@ae.gatech.edu) [eric.lynch@gatech.edu](mailto:eric.lynch@gatech.edu)  
Daniel Guggenheim School of Aerospace Engineering  
Georgia Institute of Technology, Atlanta, GA 30332-0150, USA

and

Richard E. Brown  
[rbrown@eng.gla.ac.uk](mailto:rbrown@eng.gla.ac.uk)  
Department of Aerospace Engineering, University of Glasgow  
Glasgow, G12 8QQ, UK

## Abstract

Accurate first-principles flow prediction is essential to the design and development of rotorcraft, and while current numerical analysis tools can, in theory, model the complete flow field, in practice the accuracy of these tools is limited by various inherent numerical deficiencies. An approach that combines the first-principles physical modeling capability of CFD schemes with the vortex preservation capabilities of Lagrangian vortex methods has been developed recently that controls the numerical diffusion of the rotor wake in a grid-based solver by employing a vorticity-velocity, rather than primitive variable, formulation. Coupling strategies, including variable exchange protocols are evaluated using several unstructured, structured, and Cartesian-grid Reynolds Averaged Navier-Stokes (RANS)/Euler CFD solvers. Results obtained with the hybrid grid-based solvers illustrate the capability of this hybrid method to resolve vortex-dominated flow fields with lower cell counts than pure RANS/Euler methods.

## Nomenclature

$C_T$	thrust coefficient
$n$	iteration number
$\underline{n}$	unit surface normal vector
$\mathbf{q}$	flow state
$R$	rotor radius
$\underline{R}$	coordinate vector
$S$	surface
$\underline{S}$	vorticity source term
$t$	time
$\underline{u}$	velocity field
$u_\infty$	free stream velocity field
$V$	volume
$\nu$	viscosity
$\rho$	air density
$\rho$	source point coordinate vector

$\underline{\omega}$	vorticity vector
$\Omega$	rotor rotation rate
$\Omega$	coupling interface region

## Introduction

Accurately determining the fluid dynamic environment is critical to the calculation of rotorcraft performance. Since the helical wake usually remains near the rotor blades for an appreciable amount of time, inaccurate or diffusive wake modeling also leads to poor predictions of blade loading and BVI events so that correct prediction of the wake strength, structure and position is essential. Both Lagrangian vortex methods and grid-based Computational Fluid Dynamics (CFD) techniques have been developed to numerically simulate rotor wake flows; however, while such analysis tools are capable of predicting the loading on rotors under various flight conditions, formulational assumptions or computational cost constrain their routine application to general configurations.

---

Presented at the American Helicopter Society 66<sup>th</sup> Annual Forum, Phoenix AZ, May 11-13, 2010. Copyright © 2010 by the American Helicopter Society International, Inc. All rights reserved.

Historically, rotor blade aerodynamics have been modeled with vortex methods of varying sophistication (lifting line, lifting surface etc), however these methods

are limited in their ability to address viscous and compressible flow. While extensions of these methods can address compressibility and viscous effects to a limited degree, only Navier-Stokes CFD solvers are capable of reproducing all of the significant fluid dynamics mechanisms and producing predictions of sufficient engineering accuracy for both steady and unsteady blade loading [1-3].

Lagrangian free-wake methods, where the rotor wake is modeled as a vortex filament (or a collection of vortex filaments) trailed from each blade, can predict adequately the wake induced loading on a rotor for a variety of flight conditions and applications [4-11]. Such methods offer fast turnaround times, even real-time, and can be easily coupled to lifting-line and panel methods. While these approaches are ideally suited to propagating vortices over long distances and offer a compact flow description, their efficiency deteriorates for flight conditions where the rotor wake undergoes large scale distortions (e.g. strong wake on wake interactions such as vortex ring state, airframe interactions, and ground effect). In such situations, the neglected viscous and compressibility effects are likely to become significant. Also, core distortions become pronounced and must be modeled empirically.

Traditional grid-based CFD methods (i.e., solution of the density, velocity and pressure variables), do not make any a-priori assumptions about the shape and evolution of the flow-field. These techniques are, in principle, capable of modeling the formation, evolution, coalescence and rupture of the complete rotor wake. Unfortunately, because of the helical/epicycloidal nature of the rotor wake, regions of strong vorticity remain near to the rotor for appreciable amounts of time, and the extended action of numerical diffusion, inherent in current differencing methods can quickly smear the vorticity without expensive grid refinement [12].

The ability to preserve intense vortices and other localized flow features in rotorcraft flow-field calculations remains a major challenge, and many researchers have tried to solve the numerical diffusion-induced problem, with limited success, by increasing both the grid resolution and the accuracy of the numerical technique used to transfer flow properties from one grid cell to the next [13-20]. Vorticity Confinement [21-25] can also be added to the CFD formulation, but results are highly sensitive to parameter settings [23].

Attempts have also been made to combine the best features of CFD and vortex filament techniques [26-35] and whilst these coupled solutions generally yield improved performance predictions for a select number of flight conditions, they still suffer from numerical diffusion of the rotor wake, particularly near the blade

tip in the region where the wake has not rolled up sufficiently to start the Lagrangian solution [26, 36-38]. In addition, these techniques have difficulty modeling flight regimes where vortices pass close to the rotor blade [28, 35, 39].

Lagrangian particle methods have also been coupled to CFD tools to address the diffusion of vorticity [40, 41]. These methods typically suffer from the same limitations as their filament based counterparts, which is expected since vortex particles are functionally equivalent to very short filament segments. Furthermore, while particle methods have been very successful at solving two-dimensional problems, difficulties associated with maintaining divergence-free vorticity fields and managing particle disorder [42], preclude routine application of such methods to high Reynolds number three-dimensional flows, such as those associated with rotorcraft. Nevertheless, promising research in this area based on rotor blade beam/lifting line models is ongoing [43, 44].

Recently, it has been shown that numerical diffusion of the rotor wake can be controlled in a CFD solver – albeit, one based on a vorticity-velocity formulation – by carefully constructing the flux formula and selecting an appropriate flux limiter [45-47]. The Vorticity Transport Model (VTM), however, has not been developed to the extent where it can provide good a-priori predictions of blade aerodynamics, and is driven by a Weissinger-L panel method coupled to airfoil data tables. This limitation motivated the development of a modular flow solver, VorTran-M, initially based on the CFD solver in VTM that can be coupled to a conventional Navier-Stokes code [48, 49]. In this arrangement, the Navier-Stokes solver is used to resolve the (presumably small) regions of compressible viscous flow near to the blades, and VorTran-M is applied to the remaining, vortex dominated flow domain. Such an arrangement simultaneously exploits the ability of traditional CFD to predict local aerodynamics and the low dissipation first principles wake modeling capabilities of VorTran-M in the wake.

Building upon the prior work presented in [48-50], this paper explores concepts for accurate hybrid coupling and presents results from the integration of a velocity-vorticity solver, VorTran-M with several unstructured, structured and Cartesian based RANS/Euler CFD solvers.

## Vorticity Transport Methodology

In the hybrid strategy, the far field wake is solved using the unsteady vorticity transport equation, which has been implemented in the VorTran-M solver [48-50]. It is obtained by taking the curl of the Navier-Stokes equations. Denoting the local flow velocity,  $\underline{u}$ , and the

associated vorticity distribution,  $\underline{\omega} = \nabla \times \underline{u}$ , then for incompressible 3D flow this equation is stated as follows:

$$\frac{\partial}{\partial t} \underline{\omega} + \underline{u} \cdot \nabla \underline{\omega} - \underline{\omega} \cdot \nabla \underline{u} = \nu \nabla^2 \underline{\omega} + \underline{S} \quad (1)$$

where  $\underline{S}$  is a vorticity source representing vorticity that arises on solid surfaces immersed in the flow. For rotary wing aircraft, the wake arises as a vorticity source associated with the aerodynamic loading of the rotor blades, fuselage, wings, and other parts of the vehicle. The velocity induced by this vorticity distribution at any point in space is governed by the Biot-Savart relationship,

$$\nabla^2 \underline{u} = -\nabla \times \underline{\omega} \quad (2)$$

that, when coupled to Equation 1, feeds back the strength and geometry of the rotor wake to the loading of the rotor blades and fuselage.

VorTran-M employs a direct numerical solution to Equations 1 and 2 to calculate the evolution of the rotor wake. At the beginning of each time step the numerical implementation calculates the velocity,  $\underline{u}$ , at which the vorticity field must be advected, by inverting Equation 2 with either cyclic reduction [45, 51, 52] or a Cartesian Fast Multipole method on an adaptive grid [46, 53, 54]. The vorticity distribution is then advanced through time using a discretized version of Equation 1, obtained using Toro's Weighted Average Flux (WAF) algorithm [55] and Strang spatial splitting. This process is then repeated for each time step.

This numerical technique conserves vorticity explicitly, and has been shown to preserve the vortical structures of rotor wakes for very long times. Numerical diffusion still admits the spreading of vorticity, but this can be controlled by implementing a suitable flux limiter in the WAF scheme [56]. Such an approach is in contrast to that of [57], where a vorticity-velocity formulation is employed to conserve vorticity, however use of conventional flux limiters results in the same large cell counts (30 across a vortex) as traditional CFD to resolve vortical flow fields.

Figure 1, demonstrates the ability of this formulation to capture detail in the wake structure of a hovering rotor even with a relatively coarse grid (800,000 grid cells, 50 cells per rotor radius, 6 cells per blade chord) [49]. This example illustrates that if the vortical structures in the wake are accurately resolved, then the solution will show experimentally observed fluid dynamic phenomena such as the growth of the vortex pairing instability and the subsequent loss of symmetry in the wake downstream of the rotor.



Figure 1: Snapshot of vortex pairing in the wake beneath a two bladed hovering rotor from [53]

### Computational Fluid Dynamic Solvers

An important goal of the work presented here is to demonstrate the feasibility of successfully and efficiently implementing a hybrid arrangement in a variety of CFD solvers and to identify and address key numerical issues arising from the interface treatment. Thus, the development of a hybrid CFD/VorTran-M solver has been investigated using four distinct CFD methodologies: CDI's RSA3D (unstructured RANS) and CGE (Cartesian grid Euler) codes, as well as NASA's OVERFLOW (structured overset RANS) and FUN3D (unstructured RANS).

#### RSA3D

CDI's Rotor Stator Analysis in 3D (RSA3D) was originally developed under the sponsorship of NASA Glenn Research Center to model aeroelastic rotor-stator interaction problems, and can also analyze flows over propellers, rotors, complex multistage compressors/turbines and cascades [58-61]. RSA3D solves the RANS equations on a unstructured moving deforming grid using multigrid acceleration strategies [58]. It also includes an efficient quad-tree-based interpolation scheme to handle the sliding rotor-stator interface in a consistent and conservative manner, as well as an optional containment-dual based discretization scheme to reduce dissipation on high aspect ratio grids [59-61].

#### CGE

CDI's Cartesian Grid Euler (CGE) solver determines the three-dimensional unsteady flow field by solving the compressible Euler equations upon a Cartesian grid structure consisting of a hierarchical collection of nested cube-shaped cells (an octree) [62]. A central element in the Cartesian grid concept is reliance upon intersection methods to generate the cell volumes and areas at the surfaces rather than attempting to locally align the mesh with complex surfaces. Once a surface definition has been provided, the subsequent grid generation and flow computation can proceed autonomously since the

Cartesian mesh does not need to be boundary conforming. Moreover, while primarily intended to solve compressible flows, CGE has also been shown to behave well for low speed flows with Mach number less than 0.1.

### OVERFLOW

NASA's OVERFLOW (2.1) code [63-65] solves the compressible RANS equations on either single block or Chimera overset mesh systems for all types of grid topologies (O-, H- C-). Second-order temporal integration is achieved via dual time stepping or Newton sub-iterations. Spatial discretization options include a range of schemes from second to fifth order accuracy. Low-Mach number preconditioning is available to compute low-speed flows.

### FUN3D

The FUN3D code has been developed at the NASA Langley Research Center [66-68] to solve both compressible and incompressible RANS equations on unstructured tetrahedral or mixed element meshes. The incompressible RANS equations are simulated via Chorin's artificial compressibility method [69]. A first-order backward Euler scheme with local time stepping is applied for steady-state simulations, while a second-order backward differentiation formula (BDF) resolves time-accurate simulations. Non-overlapping control volumes surround each cell vertex or node where the flow variables are stored, resulting in a node-based solution scheme. An overset mesh capability resolves multiple frames of motion within one simulation [70].

### Hybrid Grid-Based CFD Solver Development

General and versatile interfacing strategies for coupling CFD methods to a vorticity-velocity ( $\omega$ - $u$ ) based solver have been developed that build upon commonly used techniques for coupling numerical flow solvers together, and incorporate new elements to account for grid motion and support the immersion of multiple bodies (rotor blades, rotors and/or fuselage components) in the flow.

The coupling strategy relies on the VorTran-M module for vorticity transport outside of the CFD domain and utilizes the CFD solver to handle the viscous compressible flow near the surfaces and provide the vorticity source terms required in VorTran-M.

The coupling procedure is guided by several considerations regarding the underlying formulations and capabilities of the respective codes:

1. In order to control numerical dissipation within the CFD solver at minimal cost, it is desirable to use a fine mesh over the smallest volume necessary. However, since  $\omega$ - $u$  formulations are

usually incompressible, the CFD grid must extend sufficiently far that the effects of compressibility outside the domain can be neglected.

2. In a vorticity-velocity formulation, the velocity anywhere inside a domain is completely determined by the vorticity distribution over the domain and the velocity distribution over the domain boundary.
3. In general, the CFD grid will move relative to the mesh used by the  $\omega$ - $u$  method.
4. The local flow solution is transferred from the CFD solver to the  $\omega$ - $u$  solver where it is then evolved according to the vorticity transport equation. Steps must be taken to prevent double counting of vorticity by ensuring that once the vorticity is transferred to the  $\omega$ - $u$  solver, it or its evolved derivative will not be projected again at a later time step.

### CFD/ $\omega$ - $u$ Coupling Strategies

Coupling CFD to vorticity-velocity methods requires a two-way interface (see Figure 2), which has been implemented using both direct coupling, where the CFD code calls the vorticity-velocity solver as a compiled library, and also using Python-based strategies. Several methods have been employed for hybrid coupling, and the following paragraphs review these methods and present their advantages and limitations in the context of the current application.

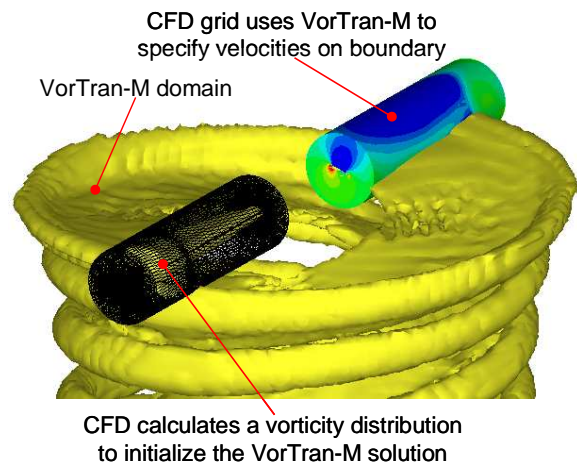


Figure 2: Schematic of multi-domain CFD/VorTran-M coupling

### Initializing the Wake Vorticity

*Loading approach:* By far the most common method for setting the vorticity in the wake based upon the CFD solver is to calculate the spanwise loading along the rotor blade and then use this to radially distribute,

circulation, and hence vorticity, in the wake [33, 35, 71]. In its simplest form the peak circulation is used to set the strength of a single vortex filament located either at the blade tip, location of peak circulation or at the centroid of circulation. More sophisticated adaptations trail multiple filaments from the blade based on the change in circulation along the span. Such an approach is relatively simple and robust and builds upon the assumption that the CFD predicted loading should provide the most accurate representation of the near wake. Unfortunately, this strategy implicitly uses a thin-wake assumption (i.e. a Kutta condition is applied so that the wake leaves the trailing edge of the blade) [33] where any vorticity related to separated flow is accounted for in terms of changes in the strength of the wake, but NOT the location (relative to the leading and trailing edges). An additional concern with this method is that without care in providing wake feedback on the CFD solution, it is possible for the near field representation to diverge from the free-wake since the CFD method and the wake approach solve different equations (i.e. viscous and compressible CFD versus incompressible inviscid free wake).

*Direct coupling:* Direct (volumetric and boundary) coupling approaches can also be employed to initialize the wake by setting the three components of vorticity based on the vorticity in each CFD cell on the cells at the outer boundary of the CFD domain (i.e. the CFD domain is discretized as one particle per CFD cell, or one filament per CFD cell). For particle methods [40, 41], care must be taken to ensure that there is sufficient CFD resolution to maintain adequate particle overlap, however for filament based approaches the situation becomes more complicated. A single filament can be trailed from each CFD boundary face based on the circulation in each cell, however determining the shed component and the filament connectivity is complicated and may result in a very inefficient wake representation (i.e. many weak filaments). Of course, some alternate representation of the vorticity interior to the boundary must be included for correct evaluation of the Biot-Savart equation. A more sophisticated application of this method is employed in the VTM code [46] and by Zhao and He [44] where the loading (albeit from a lifting line/surface style thin wake) is projected onto a temporally and spatially changing interpolation surface prior to discretization.

#### Providing Feedback to the CFD Solver

*Boundary coupling:* The simplest way to provide feedback to the CFD solver is via modifications to the outer boundary state [39, 40]. This ensures that the tip vortex trajectories predicted by the wake and CFD solvers align at the boundary. Unfortunately, this approach requires adequate resolution in the CFD domain to ensure adequate resolution to the tip vortex,

as well as sophisticated boundary conditions to prevent the spurious reflections from the interface [39].

*Perturbation Approach:* This approach attempts to decouple the flow field (i.e. the Navier-Stokes/Euler equations) into a rapidly varying vortical component that can be solved separately with a suitable wake model, and a smoothly varying part that can be accurately solved using a CFD solver that captures effects neglected by the wake model [31, 32]. Though conceptually appealing, this approach breaks down when, due to its own modeling idealizations, the wake model “drifts” from the true solution and so no longer provides a useful reference solution from which the smoothly varying part can be developed. More generally, decoupling the solution to the Navier-Stokes/Euler equations is not always possible if there are solid bodies in the computational domain because the boundary conditions do not decouple conveniently. If the wake model relies upon a Biot-Savart law to calculate the wake-induced velocity, and velocities are required at every grid point in the CFD domain, then the perturbation approach can become prohibitively expensive for 3D computations even if some sort of field based method, such as Fast Multipole or Poisson equation inversion, is employed. A variation of this approach is employed in the HELIX code, where vortex embedding is used to drive a potential flow model [26, 29, 30]. Here the physical velocity components are decomposed into a part associated with the velocity potential and a vortical part associated with regions of the flow containing the rotor wake. A Lagrangian technique is employed to model the wake, and this wake solution is then embedded into the potential flow domain by interpolating the wake induced velocity from the Lagrangian wake into the appropriate cell in the potential domain [72, 73].

*Surface Transpiration Approach:* This approach directly addresses the computational expense and generality of the perturbation approach by evaluating the rotor wake induced velocities only at those grid points that are located on surfaces immersed in the flow [74, 75]. In essence, this technique serves to implicitly alter the local angle of attack of each aerodynamic segment of along the rotor blade, and is only strictly valid for Euler calculations where no boundary layer is modeled and the velocity at the surface of the blade can be non-zero. Moreover, because the influence between the rotor wake and CFD models is essentially one-way (i.e. the wake model sets transpiration velocities in the CFD calculation, but the CFD flow solution usually has no bearing upon the wake model) the method remains limited in its ability to model the vortex distortions resulting from vortex-vortex and vortex-surface interactions.

*Field Velocity Approach:* The field velocity approach uses the techniques of indicial modeling to permit the influence of the rotor wake to alter the time metrics of the CFD grid without actually distorting the grid [28, 33, 35, 76, 77]. This is a quasi-steady type of approach that linearizes the induced velocity of the rotor wake, but neglects the effects of the wake pressure and density fields. While this technique inherently neglects second order wake effects, it is potentially more accurate than the surface transpiration method and less complex than the perturbation approach. However, like the surface transpiration approach, the field velocity technique attempts to address the boundary condition problems of the perturbation method by evaluating the rotor wake induced velocity on the surface of the rotor blade; unfortunately, this location, where the no-slip boundary condition should be enforced, is exactly where vorticity-based wake models have problems and poor predictions of the blade surface velocities may result. Additional problems may arise from double counting of the wake-induced velocity since both the CFD solver and the wake solver have solutions in the overlap region. A recent application of this approach has attempted to address this limitation by not including the induced velocity influence of the free wake in the overlap region when calculating the field velocities [33], unfortunately, given the definition of the Biot-Savart relationship, this strategy results in erroneous induced velocities.

*Hybrid Approach:* This technique is a hybrid pseudo overset approach that couples multiple separate computational domains; an inner (CFD) and an outer (wake) domain, connected by an overlap region. The outer domain serves to set the boundary conditions of the inner domain, whilst the overlap region functions as an interpolation region to determine the passage of the flow from one domain to the other. This hybrid approach addresses the shortcomings of the approaches described above by evaluating the rotor wake induced velocities in an overlap region of the flow where both the CFD and wake methods provide adequate modeling fidelity. By suitably choosing the size and location of the overlap region, this technique can be made to preserve the spatial resolution of each numerical solver and thus maintain an accurate representation of the flow passing between the two domains. Furthermore, this approach minimizes computational cost associated with having two coupled solutions since the extra evaluation of the Biot-Savart relationship is required only at the intersection of the two domains rather than throughout the two complete numerical domains as in the perturbation and field velocity approaches. Since the majority of the wake is represented in the vorticity-velocity domain, this hybrid method further optimizes the use of computational resources since it is no longer necessary to devote tightly spaced grid points in the far-

field to preserve wake vortices. The inner CFD grid can thus now be limited to the small regions about the surfaces where compressibility and viscosity are important and high resolution of vortex-vortex and vortex-surface interactions is required.

In the hybrid coupling scheme, the wake solver vorticity in a selected region is overwritten with values from the CFD solution at every time step (see Figure 2). This procedure, described in detail in [49] eliminates double counting and also facilitates the handling of moving grids, a requirement for efficient rotorcraft modeling. While other options can be considered, the overwriting procedure appears to be the most effective in simultaneously accommodating general moving grids while retaining simplicity in both formulation and code implementation.

### **VorTran-M/CFD Coupling Strategy**

These considerations motivated the current approach for rotorcraft applications that defines four regions in the flow domain and treats vorticity differently in each domain. These regions, summarized in Figure 3, are defined as:

- $\Omega_1$ : Lies inside CFD boundaries, and encloses all solid surfaces. The flow is represented entirely by the CFD solver.  $\Omega_1$ , can be disjoint, as in Figure 2, but must contain all solid bodies of interest.
- $\Omega_2$ : Surrounds  $\Omega_1$  and lies inside CFD boundaries. The flow is represented by CFD solver. The flow solution is transferred to VorTran-M at the start of every time step, thus overwriting the VorTran-M solution in this region. VorTran-M evolves the vorticity during the time step to determine the amount of vorticity that advects out of  $\Omega_2$ .
- $\Omega_3$ : Consists of the remaining CFD domain lying outside of region  $\Omega_2$ . Both VorTran-M and the CFD solver evolve the flow in the normal manner. This region is usually small, often only several cells thick, and promotes solution stability by preventing instantaneous feedback between the solvers. The VorTran-M module sets the outer CFD boundary conditions.
- $\Omega_4$ : Consists of the remaining VorTran-M domain lying outside of region  $\Omega_3$ . The flow is entirely represented by VorTran-M.

### **Time Stepping Strategy**

A time stepping strategy is defined that consists of advancing both the CFD and vorticity-velocity solutions forward in time and then overwriting the vorticity-velocity solution in  $\Omega_2$  using the CFD results.

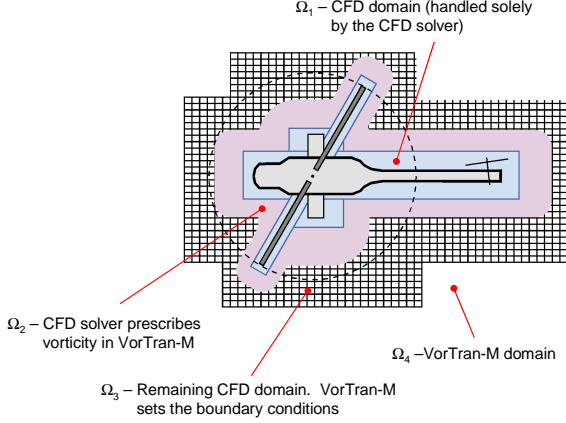


Figure 3: Detailed schematic of CFD/VorTran-M overlap regions

At time  $t^n$ , a solution in both the CFD and VorTran-M domains is available. This solution is advanced to the next time level,  $t^{n+1}$ , using the respective integration strategies. In most arrangements, an implicit time marching strategy is used in the CFD code where the discrete set of equations defining the flow field update,  $\mathbf{q}_{CFD}^{n+1} - \mathbf{q}_{CFD}^n$  are evaluated at  $t^{n+1}$ . Since VorTran-M employs an explicit scheme it is most convenient to first advance the VorTran-M solution to  $t^{n+1}$  so that the resulting flow field,  $\underline{\omega}_{VorTran-M}^{n+1}$  and  $\mathbf{q}_{VorTran-M}^{n+1}$ , are available to evaluate flow states at the CFD boundary. Once both the VorTran-M and CFD solvers have advanced the solution to  $t^{n+1}$ , the overwrite step is performed where the CFD solution in  $\Omega_2$  (which may differ from step to step) overwrites the VorTran-M solution.

### Coupling Interfaces: General Cell Intersection and Insertion

#### Application to Unstructured Grids

A direct cell intersection method (vorticity\*volume) based on the coupling strategy described above was tested via a RSA3D and VorTran-M coupling. Here, the vorticity field in the region overlap region is calculated by finite differencing the CFD solver velocity field. RSA3D uses an unstructured grid vertex based scheme to interface with VorTran-M, thus the volume integrated vorticity in a tetrahedral cell is

$$\underline{\alpha} = \int_V \nabla \times \underline{u} dV = \oint_S \underline{n} \times \underline{u} dS \cong \frac{1}{3} \sum_{k=1}^4 \underline{u}_k \times \underline{S}_k \quad (3)$$

where  $\underline{u}_k$  is the velocity at tetrahedral vertex,  $k$ , and  $\underline{S}_k$  is the outward directed area of the face opposite node,  $k$ .

The last identity follows from the identity,  $\sum \underline{S}_k = \underline{0}$ , for closed polyhedra.

For inviscid calculations, the surface velocity,  $\underline{u}_S$ , is nonzero. If one considers the inviscid result as the limiting case of a viscous calculation where the boundary layer has become infinitesimally thin, then it is clear that the boundary layer must contain vorticity in order to transition from zero velocity at the surface (no-slip condition) to  $\underline{u}_S$  at an infinitesimal height above it. The vorticity strength associated with a surface area,  $A$ , is given by:

$$\underline{\gamma}_S = \int_{V_\delta} \nabla \times \underline{u} dV = \oint_{S_\delta} \underline{n} \times \underline{u} dS = \int_A \underline{n} \times \underline{u}_S dS \quad (4)$$

where  $V_\delta$  is the infinitesimal volume occupied by the vorticity sheet of thickness,  $\delta$ , lying upon the area,  $A$ ;  $S_\delta$  is the bounding surface of  $V_\delta$ . For moving surfaces it is also necessary to compute a ‘‘source’’ term:

$$\underline{\beta}_S = \int_A \underline{n} \cdot \underline{u} dS \cong \frac{1}{3} A \times \sum_{k=1}^3 \underline{u}_k \quad (5)$$

Other than its inherent discrete approximations, the Biot-Savart relation provides a complete description of the flow field provided that  $\underline{\alpha}$  and the surface velocities are known.

A finite wing configuration, summarized in Table 1, provided a useful first test for the hybrid RSA3D/VorTran-M arrangement. Calculations were performed on different grids having identical chordwise resolution (128 mesh points about the airfoil), but varying outer boundary placements. The smallest grid extends only 1.5 chord lengths away from the blade surface, which by conventional CFD standards would be considered far too small for reliable results. The large grid is more typical and extends 10 chords away from the surface. In all cases, a smoothly varying mesh is obtained by constraining the grid spacing to grow no faster than by a factor of 1.1 from element to element. For the hybrid calculations, the finest VorTran-M mesh spacing is set to 2% span (18% chord) which is about twice the free-stream convection distance in a time step (i.e., CFL=0.5) thus ensuring a stable VorTran-M calculation using its explicit time marching method. The Courant numbers for the finest mesh cells on the CFD side are significantly greater than 1.0 and implicit time stepping is necessary in RSA3D.

The wing, at  $8^\circ$  angle of attack, is impulsively started from rest and thus generates a start up vortex at the trailing edge. This vortex convects downstream and connects to the wing via two streamwise trailing vortex

structures located near to the wing tips, see Figure 4. These vortex structures lower the lift coefficient in a time dependent manner. Inviscid, low Mach number flow and small flow angles are assumed thus allowing comparison to classical theories.

Table 1: Fixed wing parameters

Profile	NACA 0012
Aspect Ratio ( $AR$ )	8.8
Mach Number ( $M_\infty$ )	0.2
270K Cell Mesh	$x \in (-1.5c, +2.5c)$
492K Cell Mesh	$x \in (-10.c, +11c)$

Estimates for the 3D lift coefficient,  $C_{L3D}=a_{3D}\alpha$  for the NACA 0012 airfoil in inviscid flow were drawn from several sources. The steady state 2D and 3D lift curve slopes,  $a_{2D}$  and  $a_{3D}$ , are approximately (for non-elliptic wings) connected by the aspect ratio according to:

$$a_{3D} = \frac{a_{2D}}{1 + \left( \frac{a_{2D}}{\pi AR} \right) (1 + \tau)} \quad (6)$$

where for the case presented here  $\tau=0.2$  [78]. XFOIL [79] predicts,  $C_{L2D}=0.9957$  at  $M_\infty=0.2$ , which translates to  $C_{L3D}=0.7603$ . Inviscid calculations with the RSA3D code using a fine grid extending 10 chords upstream and downstream from the surface predict  $C_{L3D}=0.7573$ , which agrees closely ( $\sim 0.4\%$ ) with the XFOIL prediction.

Figure 4 shows the developing wake structure obtained with the hybrid RSA3D/VorTran-M including the starting and trailing vortices. The most striking observation is the preservation of the starting vortex as it traverses the VorTran-M mesh. The ability to sustain this vortex poses a challenge for any Eulerian formulation because it varies rapidly in both space and time. The trailing vortex structures on the other hand also vary rapidly in space, but for this problem steady state conditions near the wing are achieved that do not exhibit significant temporal variation. The ability to resolve the starting vortex multiple spans downstream without significant dissipation attests to VorTran-M's inherent strength when applied to vortex dominated flow problems. The CFD code on the other hand is unable to preserve this vortical structure because of numerical diffusion on this grid. Temporally growing wavy perturbations can be observed along the trailing vortices suggesting an aerodynamic instability. Twisting striations in the trailing filaments are also

evident and are consistent with the locally induced swirl.

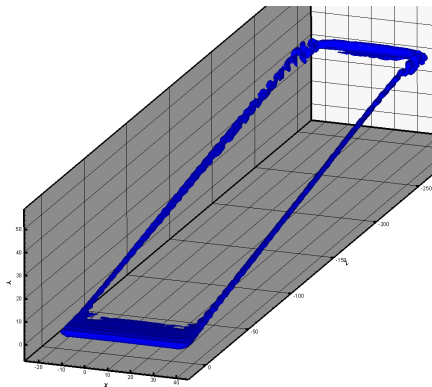


Figure 4: Perspective view of the developing wake structure for an impulsively started wing. All iso-surfaces are drawn at the same vorticity magnitude.

The steady state lift coefficients obtained with the various grids are summarized in Table 2. The main observation from this table is that the use of the VorTran-M considerably improves the predicted lift coefficient for the reduced domain CFD meshes. For example, the lift predicted with the hybrid method on the small extent mesh (270,000 cells, outer boundaries located 1.5 chords from the surface) agrees with the large domain CFD and XFOIL predictions to within 1.1% error. Without the VorTran-M module to represent the flow outside the CFD domain, the error is 5.7%. Generally, the CFD predictions on the truncated mesh tend to overestimate the lift coefficient compared to the large mesh CFD results, and this is because truncating the wake eliminates the influence of the downstream wake, thus reducing the induced downwash and increasing the effective angle of attack. These results show that not only is the vorticity being correctly transferred from RSA3D to VorTran-M solutions, but the influence of this convecting wake is being fed back properly to the RSA3D solution via the outer boundary conditions.

Table 2: Computed steady state lift coefficients

Mesh/Case	VorTran-M	$C_L$
270 Cell Mesh	No	0.8039
492 Cell Mesh	No	0.7573
270 Cell Mesh	Yes	0.7688
Flat Plate	N/A	0.7004
XFOIL	N/A	0.7603



A bluff body wake is considered next. Unlike the relatively thin wakes shed from aerodynamically clean surfaces, bluff body type flows are dominated by unsteadiness and periodically shed vortical structures. Simulating such flows serves to demonstrate the hybrid code's abilities to reliably predict the spatial and temporal structure of the wake.

The wake structure and characteristic shedding frequencies are strongly influenced by the feedback (in terms of induced velocities) of the wake upon the fixed surfaces. Reliable prediction of these structures therefore is contingent upon the accurate transmission of wake-induced velocities at the outer boundaries back to the body.

The bluff body simulations consisted of orienting the wing described in Table 1 at 90° angle of attack and impulsively starting the calculation with  $M_\infty=0.2$ . The RSA3D/VorTran-M calculation was carried out using the 270,000 tet. grid used earlier and a near grid VorTran-M spacing of 18% chord. While the grid would be too coarse for resolving features near the surface, it appears adequate for capturing the wake dynamics further downstream.

The wake after 1800 time steps, when the wake has convected approximately 67 chords downstream, is shown in Figure 5. By this point a periodic vortex shedding process is fully established with spanwise vortices of approximately equal and opposite vorticity being generated successively off the trailing and leading edges. The near wake exhibits intricate linking structure and strong three-dimensional features which are attributed to end-effects that must arise to enforce the Helmholtz constraint (i.e., vortices cannot terminate in the flow so that each of the strong spanwise vortices must link to one or more of its oppositely oriented neighbors via streamwise connecting vortices to form closed loops of vorticity). Further downstream, the vortex induced stretching and subsequent inter-linking results in finer scale structures. The numerous eddies tend to cancel each other so that their net far-field influence becomes small. This implies that in CFD calculations it is only necessary to resolve the nearest portions of the wake where the larger vortex structures dominate the wake-induced contributions back on the shedding body.

Sample force time histories are presented in Figure 6 below. The fluctuations are induced by the vortex street associated with periodic wake shedding that occurs as the flow passes the wing. The force history reflects the overall evolution of the flow beginning with formation of the starting vortex that then convects downstream while symmetry in the wake breaks thus leading to the three-dimensional vortex street.

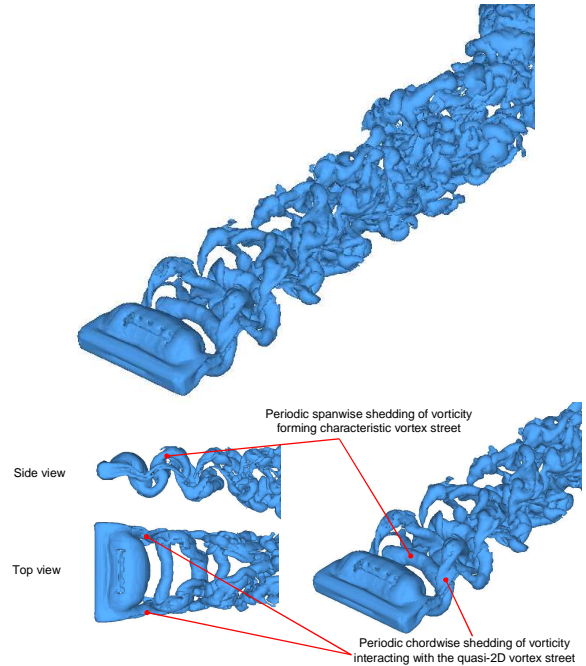


Figure 5: Wake geometry expressed as vorticity iso-surface for the rectangular wing positioned normal to the flow

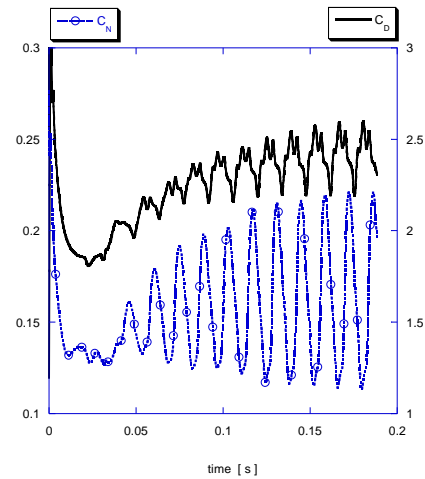


Figure 6: Force time histories for a wing at 90° angle of attack predicted by hybrid RSA3D VorTran-M code. Solid lines: lift coefficient, dashed lines: drag coefficient

A non-dimensional gauge of the vortex shedding frequency behind a bluff body is the Strouhal number,

$$St = \frac{fL}{V} \quad (7)$$

where  $f$  is the number of vortices formed (on one side of the vortex street) per unit time,  $L$  is the characteristic width of the body (in this case the chord length) and  $V$  is the flow velocity. The Strouhal number is governed by the interaction between three processes: (i) the generation of shed vortex structures at the bluff body

edges; (ii) the evolution of the shed vortex wake geometry and (iii) the influence of the shed wake back upon the shedding body. For flow over a wing oriented perpendicular to the flow, the Strouhal number should be  $St=0.2$  [80].

The force history shown in Figure 6 exhibits a periodic behavior with characteristic frequency  $f=71.4\text{Hz}$  which corresponds to a Strouhal number of  $St=0.2003$ . The drag response contains higher harmonics which is not surprising in light of the multiple 3D structures seen in Figure 5. The lift (normal force,  $C_N$ ) response is dominated by the first harmonic and contains a bias away from zero due to asymmetry (the NACA 0012 airfoil is not symmetric about the mid-chord plane).

The hybrid RSA3D/VorTran-M code is thus able to reproduce the oscillatory response at close to the expected frequency using a coarse, limited-extent mesh and a small fraction of the computational resources required for a pure CFD computation.

Unlike the fixed wing calculations above, rotorcraft flow fields pose unique challenges for traditional CFD solvers because the wake retains its strength and remains near the rotor for long periods. Performing such calculations with RSA3D/VorTran-M serves to illustrate the long-term vorticity preservation capabilities of the model. Furthermore, the vorticity shed from a rotor can re-enter the CFD domain of the subsequent blade. This raises a new challenge for hybrid modeling, namely the ability to transmit re-entrant vorticity that convects from the outer VorTran-M domain into the CFD calculation across the CFD outer boundary.

Slow speed ascent and high speed forward flight ( $\mu=0.325$ ) simulations were performed using a rotor similar to the active elevon rotor experiments of Fulton [81], however, to expedite turnaround time a two-bladed (rather than the original four-bladed) version of the rotor was simulated. A VR-12 profile was adopted, which is freely accessible and similar to the VR-18 cross-section actually used in the test. The blade twist gradient was  $10^\circ/\text{R}$ . Each blade grid was generated by sweeping a 2D triangular grid along the span with 128 nodes about the chord and 16 intervals along the span. The root section ( $r=56.3\text{ cm}$ ) is open and the mesh boundary on this section is treated as an outer boundary allowing both incoming and exiting relative flow. One consequence of this modeling approximation is that it suppresses the formation of a root vortex. The grid associated with each rotor blade contains 72,000 points and the grids are completely disconnected. Therefore all interactions and coupling between the blade flow fields must be effected through the vortical solution convected in VorTran-M. These calculations therefore

demonstrate both the moving mesh and multiple domain capabilities of the hybrid RSA3D VorTran-M code.

In each case shown in Figure 7 the rotation rate was 1070 RPM and no trimming of the rotor was attempted. The collective was fixed such that the tip angle of attack in hover was  $11^\circ$ . Both predictions showed excellent preservation of the rotor wake.

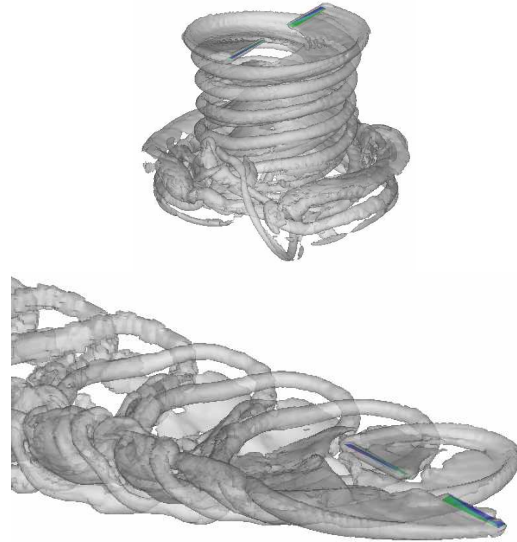


Figure 7: RSA3D/VorTran-M rotor wake predictions: two bladed untrimmed rotor in slow speed ascent (upper) and two bladed untrimmed rotor in forward flight (lower)

#### Application to Cartesian-Grids

The same direct vorticity\*volume insertion method as with RSA3D, was evaluated in CGE/VorTran-M. Here cell intersection was trivial by enforcing exact alignment between the CGE and VorTran-M cells (see Figure 8).

The CGE/VorTran-M methodology resulted in the *first* commercial ship wake database for a real-time tactical flight simulator [62]. This effort, for the US Navy's MH-60R/SH-60B tactical operational flight trainers, included over 192 ship/flow condition combinations, with the wake flow field sampled at  $\leq 1\text{m}$  spacing out to 4 ship lengths downstream.

Despite the limitations of the application of an Euler formulation near to the deck of the ship, predictions compared well with scale model and full scale ship airwake measurements (see [62] for more details). A sample ship airwake prediction is shown for a LPD-4 class ship in Figure 9 and exhibits a similar cascade in vortical scales as the wing at  $90^\circ$  angle of attack described earlier.

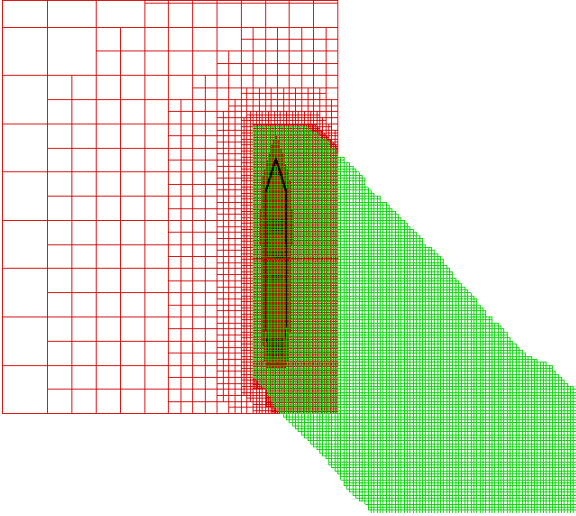


Figure 8: Intersection of Cartesian grid (red) and VorTran-M grid (green) at right for a yawed flow condition

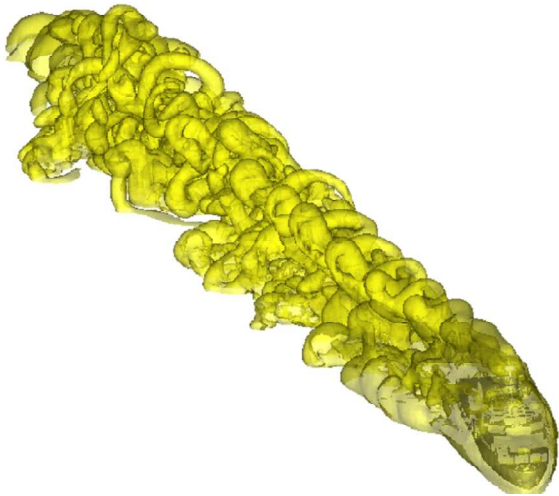


Figure 9: CGE/VorTran-M prediction of a LPD-4 class ship airwake

### Application to Structured Grids

Given the positive results obtained using the simple vorticity insertion method in the CGE/VorTran-M, a similar vorticity-based technique was examined [50] using the NASA OVERFLOW (2.1ab) structured overset solver.

Predictions for a single-bladed rotor configuration in forward flight are presented in Figure 10 through Figure 12. The rotor configuration consisted of a modified NACA 0012 airfoil section (O-grid with  $91 \times 89 \times 31$  cells) and two end caps ( $67 \times 39 \times 41$  cells each). A body of revolution representing a rotor hub ( $71 \times 121 \times 37$  cells) was also included in the analysis. To facilitate the vorticity-based coupling a non rotating outer rectangular grid domain ( $271 \times 271 \times 52$  cubic cells with  $\Delta s \approx 0.22c$ ) containing the entire rotor system was used to calculate the vorticity required by VorTran-M.

Pure OVERFLOW results are presented that utilized an off-body grid system where the grid levels coarsened by a factor of two between the near-field of the rotor system to the far field region of the computational domain. For the hybrid OVERFLOW/VorTran-M case where the OVERFLOW outer near body grid was used to input the vorticity for VorTran-M, the finest cell size in the VorTran-M domain was then set to twice the size of the near body grid ( $\Delta s \approx 0.43c$ ) cell, and the subsequent grid coarsening occurred at every rotor radius downstream.

Results are presented in Figure 10 after 2550 time steps ( $\sim 630$  degrees) when the starting vortex has convected approximately one diameter downstream. Here, the extent of the OVERFLOW near body grids is outlined in red and the active VorTran-M grid in blue. On these grids, the pure OVERFLOW computation is normally dissipative in nature and hence unable to preserve significant vorticity in the rotor wake beyond approximately one rotor revolution. The coupled OVERFLOW/VorTran-M solution, on the other hand, is able to preserve the entire wake flow, including the starting vortex, see Figure 10.

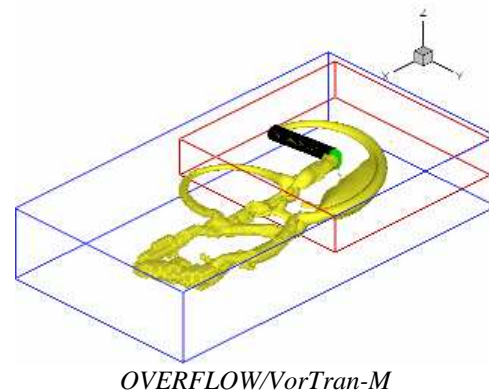
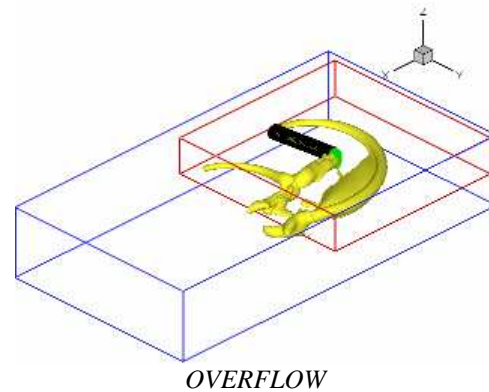
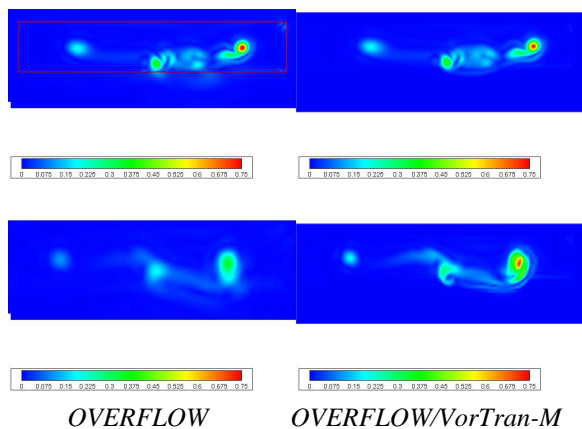


Figure 10: Predictions of wake vorticity, plotted at the same level of vorticity magnitude, for a 1-bladed rotor in forward flight after 2550 time steps

A direct comparison of the predicted vorticity field (non-dimensional OVERFLOW units scaled by the

speed of sound) for these two solutions is shown on the slices, perpendicular to the direction of flight, downstream of the rotor plane, in Figure 11 and Figure 12.

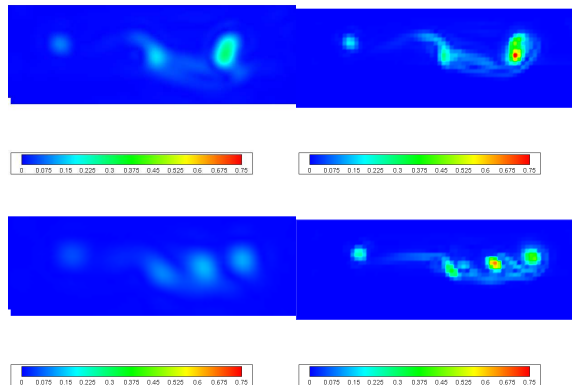
Figure 11 top compares the predictions on a slice 23.2 chord lengths aft of the rotor hub, and, despite the two-fold difference in cell size between the OVERFLOW near body grid (the red box in Figure 11 upper left) and VorTran-M, both show almost identical vorticity fields (peak vorticity for both cases is 0.77). Further downstream, 31.7 chords lengths (Figure 11 bottom), the solutions start to diverge with the OVERFLOW predicting a peak vorticity (0.36) that is half the OVERFLOW/VorTran-M value (0.72). By 33.3 chord lengths downstream (Figure 12 top), the VorTran-M grid for the hybrid calculation has been coarsened to twice the resolution of the corresponding OVERFLOW grid, yet the solution clearly demonstrates a high degree of the conservation of the peak vorticity. It is important to mention that the OVERFLOW solution has diffused the rotor blade tip vortex to a magnitude of 0.29 peak value, whereas the hybrid solver predicted a distinct core structure with peak of 0.79. Similar trends are shown at 40 chord lengths downstream in Figure 12 bottom, where the OVERFLOW predicted peak vorticity has been diffused to about 20% the value of the hybrid OVERFLOW/VorTran-M solution on a grid that is twice as coarse.



*OVERFLOW*      *OVERFLOW/VorTran-M*  
 Figure 11: Predicted vorticity magnitude for a 1-bladed rotor in forward flight on a plane perpendicular to the direction of flight, 23.2 (upper) chord lengths and 31.7 (lower) downstream of the hub.  $\Delta s_{\text{OVERFLOW}}$  (red region at left)  $\approx 0.22c$ ,  $\Delta s_{\text{OVERFLOW}} \approx 0.43c$  and  $\Delta s_{\text{VorTran-M}} \approx 0.43c$

The OVERFLOW/VorTran-M coupling presented above uses simple vorticity injection to initialize the VorTran vorticity sources. This works well when the grids are nicely aligned, but very poorly when they are not due to interpolation errors. These errors can be remedied by using a fine CFD grid, surrounding all

bodies in the flow, but this option results in high (dominant) computational cost associated with this grid. Another option is to implement formal cell intersection routines, as with RSA3D; however such methods are complicated, invasive and expensive.



*OVERFLOW*      *OVERFLOW/VorTran-M*  
 Figure 12: Predicted vorticity magnitude for a 1-bladed rotor in forward flight on a plane perpendicular to the direction of flight, 33 (upper) chord lengths and 40 (lower) downstream of the hub.  $\Delta s_{\text{OVERFLOW}} \approx 0.43c$  and  $\Delta s_{\text{VorTran-M}} \approx 0.87c$

### Coupling Interfaces: Velocity-Based Coupling Method

#### Application to Structured Grids

To address these deficiencies a more general velocity-based coupling that builds upon the observations defining flows in terms of vorticity and velocity was developed. Here, the velocity, rather than vorticity, was passed from the CFD code to VorTran-M at the VorTran-M cell corners in the overlap region. Within VorTran-M, the vorticity field was calculated by appropriately finite differencing the velocity field. This procedure can be facilitated by setting up a near body grid in a structured mesh that is identical to the finest VorTran-M grid. When implemented for use with OVERFLOW, the OVERFLOW solver treats this grid like any other, and automatically performs grid motion and hole cutting as the blades rotate, flap and, in the case of aeroelastic calculations, deform. The VorTran-M interface then uses this information to account for VorTran-M cells that intersect the body using a modified version of method described in [82]. At the end of each time step VorTran-M sets the OVERFLOW grid boundary conditions at the outer edge of this grid, or on other grids in the solution.

Sample predictions from [50] for the 8° collective, 1250 RPM Caradonna and Tung [83] hover experiments are summarized below. The two bladed zero twist rotor was meshed with three C-grids per blade (blade: 311 x 83 x

81 cells with  $y=0.955$ , tip and root caps  $85 \times 79 \times 61$  cells) and a body of revolution hub. The two bladed rotor was then surrounded by the VorTran-M grid with cells of  $\Delta s \approx 0.13c$ . VorTran-M set the boundary conditions on an additional grid of cubic cells with  $\Delta s \approx 0.13c$  ( $112 \times 58 \times 36$  cells that rotates with and encloses the rotor system, see Figure 13). After approximately 6000 time steps, this results in a total of 7.2 million active cells.

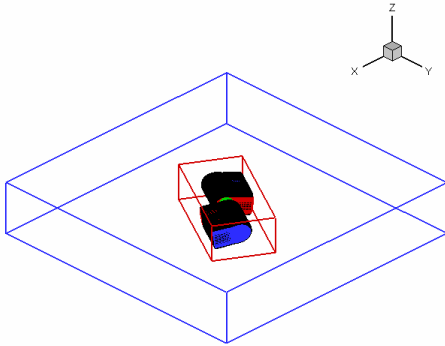


Figure 13: 2-bladed rotor and hub grid arrangement. Blade grids (black), tip-caps (blue), root-cap (red), hub grid (green), bounds of initial VorTran-M grid (blue line) and grid on which VorTran-M sets boundary conditions (red line)

A close up of the rotor wake in the near-body region predicted with pure OVERFLOW<sup>†</sup> and with the coupled OVERFLOW/VorTran-M is plotted in Figure 14, where OVERFLOW alone predicts very little root vorticity and significantly diffuses the tip vortices after about  $\psi \sim 135^\circ$ . Conversely, OVERFLOW/VorTran-M predicts significant loading along the entire span of the blade, with the tip vortices cleanly exiting the near-body region. The lack of inboard vorticity predicted by OVERFLOW also manifests itself in the rotor thrust coefficient and blade loading shown in Figure 15. OVERFLOW predicts the magnitude of the loading near to the tip, but significantly underpredicts the loading inboard of  $0.8R$ . The integrated thrust coefficient for this case was  $C_T = 0.00432$ , or 94% of the experimental value. OVERFLOW/VorTran-M more accurately reproduces the thrust coefficient ( $C_T = 0.00458$ , or 99.6% of the experimental value) and the inboard loading. However, the  $0.5R$  is still somewhat underpredicted, though this may be due to the relatively low number of revolutions simulated in these predictions. Nevertheless, the improved ability of OVERFLOW/VorTran-M to predict the spanwise

<sup>†</sup> Pure OVERFLOW predictions were undertaken on the same near-body grid arrangement as the hybrid OVERFLOW/VorTran-M. Automatic off-body grid generation was used with a factor of 2 spacing that resulted in a grid with 19.8 million cells.

loading for this hovering rotor configuration on this non-optimized relatively coarse grid is significant.

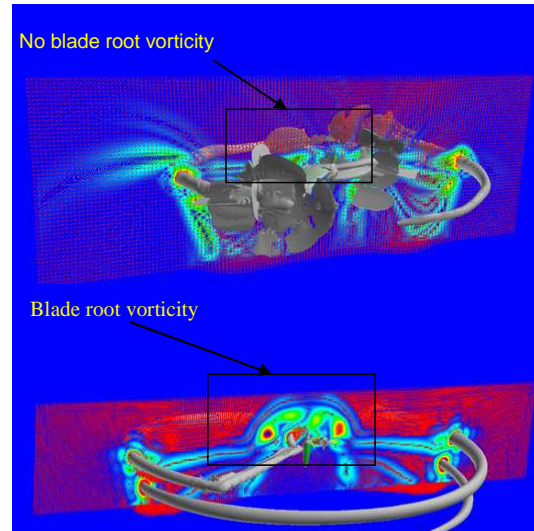


Figure 14: Close-up of OVERFLOW (upper) and OVERFLOW/VorTran-M (lower) predictions of the near-body wake and velocity vectors on a slice through the rotor from [50]

Predictions of the tip vortex trajectory are compared to experimental measurements in Figure 16 where the error bars represent the error associated with locating the center of the tip vortex (i.e. local grid cell size). Wake trajectory data was extracted from the pure OVERFLOW prediction for the first  $270^\circ$ , after which the predicted vorticity was insufficient to identify discrete vortices. Plotting Q-criterion may aid tip vortex identification, however all results presented here are based on iso-surface of vorticity magnitude.

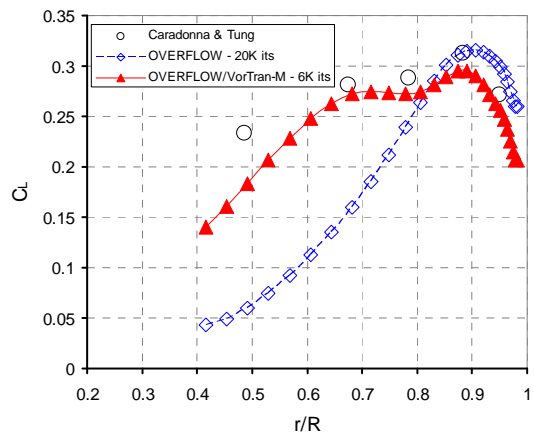


Figure 15: Comparison of measured and predicted spanwise loading ( $C_{T \text{ Experiment}} = 0.0046$ ,  $C_{T \text{ OVERFLOW}} = 0.00432$ ,  $C_{T \text{ OVERFLOW/VorTran-M}} = 0.00458$ ) from [50]

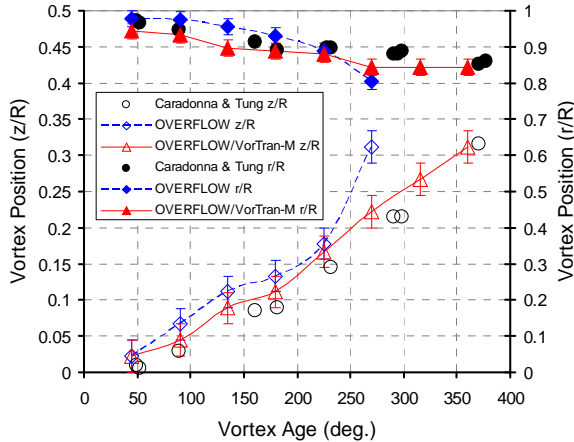


Figure 16: Comparison of measured and predicted tip vortex trajectory

Both solutions correctly predict the first  $45^\circ$  of tip vortex evolution; for the next  $180^\circ$ , however OVERFLOW predicts a tip vortex trajectory that is more outboard and lower than the measured data. Once significant wake interactions take place to distort the tip vortices (after  $180^\circ$  tip vortices start to interact with the next blade), OVERFLOW predicts a significant increase in both the descent and contraction rates. OVERFLOW/VorTran-M, correctly predicts the tip vortex trajectory for the entire revolution, with both the vertical and radial position of the wake closely tracking the experimental data throughout. OVERFLOW/VorTran-M also correctly predicts the asymptotic extent of radial contraction.

It should be noted, that in general the grids use for the pure OVERFLOW calculation would be too coarse and non-optimal, by themselves, for reliable hover calculations. Consequently, the calculations presented here do not represent the best that OVERFLOW can do; rather they serve as a simple industrial scale baseline against which to compare the hybrid OVERFLOW/VorTran-M.

### Application to Unstructured Grids

The preceding strategy was utilized to couple VorTran-M to NASA's FUN3D code. Since the vorticity distribution is inferred from the velocities evaluated over a small sub-set of VorTran-M cells (those lying in the overlap region,  $\Omega_2$ ) all that is necessary is to determine the FUN3D velocity at the cell corners of these VorTran-M cells.

Implementing such a velocity-based coupling requires that routines to interpolate velocities exist and that the surface definition (and/or suitable cell blanking information as in OVERFLOW) be made available to helper routines so that we can mark VorTran-M cells that are in the overlap region. Determining the FUN3D

velocity at the VorTran-M cell nodes can be performed efficiently (i.e. only one loop over the FUN3D grid). VorTran-M cells that have nodes inside the body can be made to take into account the bound vorticity (see [82] for more details). Similarly, since the overlap region can be defined in terms of VorTran-M cells, the VorTran-M nodes that are exterior to the FUN3D overlap region are not used.

Marking of the VorTran-M cells to calculate the overlap regions etc is performed at each time step. First the cells that intersect the surface are marked, and then based upon the desired size of the overlap and buffer region, cells are marked radially outwards away from the surface.

A sample FUN3D/VorTran-M prediction for the finite wing at  $90^\circ$  angle of attack calculated using this strategy is presented in Figure 17, along with pure FUN3D results on the same near-body grid. For this flow condition, the flow field is highly unsteady and dominated by vorticity shed and trailed from the leading and trailing edges of the wing. The flow field predicted by FUN3D (with a Spalart-Allmaras turbulence model) is shown in Figure 17 left, and exhibits separation from the upper and lower surfaces, with some wake shedding that is rapidly dissipated due to inadequate resolution in the downstream grid. In contrast, the hybrid FUN3D/VorTran-M prediction (Figure 17 right) using identical near-body mesh resolution shows a significant improvement in realism, comparable to RANS-LES predictions [84], with distinct vortices being shed from the surface, and propagated downstream.

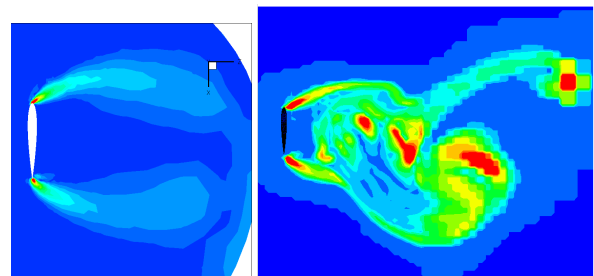


Figure 17: Mid-plane vorticity magnitude predicted by the FUN3D/VorTran-M coupled simulation for the NACA0012 wing at  $90^\circ$  angle of attack

### Lessons Learned

Three mixed element grid-based coupling interfaces have been implemented and assessed for various fixed, rotary and bluff-body configurations:

1. Cell intersection and insertion
2. Centroid-based vorticity\*volume insertion
3. Velocity-based insertion

In formal cell intersection, exact intersections of cubic VorTran-M cells and the CFD grid (for the cases presented here, the tetrahedra in an unstructured mesh see Figure 18 left), are developed and the intersection volume employed to transfer the vorticity calculated in each cell to the appropriate intersecting VorTran-M cells. Tests are also conducted to determine if the VorTran-M cells intersect the boundary or surface. This is necessary for Euler calculations to account for the “bound” vorticity associated with the surface slip velocity. Formal intersection is expensive, and requires extensive modification of the host CFD solver to determine the vorticity in each cell. Moreover, calculating the vorticity in the boundary layer (Figure 18 right), where a large fraction of the total CFD grid resides, is a computational bottleneck<sup>‡</sup>. Despite this computational cost and the required code modifications, results obtained with this method implemented within the constructs of RSA3D/VorTran-M were excellent.

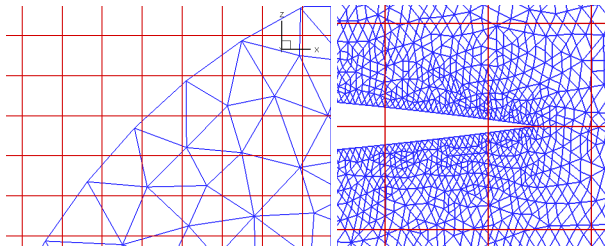


Figure 18: Intersection of unstructured (blue) and VorTran-M grids (red) at left and center

To address these costs, a simplified approach was developed and tested out in the coupling of VorTran-M to the Cartesian grid solver CGE. Here, the volume-weighted vorticity (i.e. vorticity\*volume) was calculated in overlapping cells and passed to VorTran-M at the cell centroid (see Figure 8). This method obviates the need for a formal intersection calculation since the grids coincide exactly (e.g., in the lower right portion of the red grid in Figure 8) and ensures conservation of the volume-integrated vorticity between the two codes. Again, surface bound vorticity is inserted into any intersecting cells. When coupled with the CGE, results were good.

Centroid-based vorticity insertion worked well for coupling to CGE and indeed certain OVERFLOW configurations because the CFD and VorTran-M grids can be made to align exactly and/or tight control can be placed on the size of the CFD cells in the overlap region. This is generally not the case for unstructured grids, or overset structured grids when the VorTran-M cell size approaches, or is smaller than that of the near-

body grids and discontinuous vorticity distributions generally result.

A general coupling approach that eliminates these complexities, computational costs and large interpolation errors can be obtained by reformulating the coupling in terms of velocities evaluated at the vertices of a subset of the VorTran-M cells. This approach is efficient since resolution is now determined by the target VorTran-M mesh size. It is simpler since complex and invasive volume intersections are replaced by velocity interpolation procedures that are both simpler and often available in the host code. Finally significant cost savings, with no reduction in accuracy, can be attained by careful placement of the overlap regions.

## Conclusions

This paper describes ongoing couplings between VorTran-M and several unstructured and structured grid Reynolds Averaged Navier-Stokes CFD solvers (CDI’s RSA3D, NASA’s OVERFLOW and FUN3D) and CDI’s CGE Cartesian grid solver with the goal of improving predictions of vorticity dominated flows by eliminating the diffusion issue that limits the application of pure Navier-Stokes/Euler solvers. Three coupling procedures have been described, along with sample results and lessons learned. The results presented here demonstrate improved wake and loading predictions.

## Ongoing and Future Work

Work to date has focused on developing and demonstrating the feasibility a prototype hybrid CFD/VorTran-M flow solvers. Ongoing work seeks to improve the efficiency of the coupling in addition to further validation of the approach. It is anticipated that future work will investigate developing a parallel VorTran-M module, as well as refining the fundamental module coupling strategy to facilitate interfacing to a variety of CFD solvers.

## Acknowledgements

The authors wish to acknowledge the support of the US Army Aero Flight Dynamics Directorate at Ames Research Center, specifically Mr. Mark Potsdam and Dr. Chee Tung, who guided the initial VorTran-M development and early OVERFLOW coupling work through the Small Business Innovative Research (SBIR) Program. Additional thanks also Dr. Doug Boyd and the FUN3D development team for their support in undertaking a preliminary coupling to FUN3D under a NASA SBIR Phase I effort.

## References

1. Dietz, W., L. Wang, Y. Wenren, F.X. Caradonna, and J. Steinhoff. "The Development

<sup>‡</sup> this is true of both velocity and vorticity-based coupling and is controlled by the placement of  $\Omega_2$ .

- of a CFD-Based Model of Dynamic Stall." *American Helicopter Society 60th Annual Forum*. 2004. Baltimore, MD.
2. Smith, M.J., T.-C. Wong, M. Potsdam, J. Baeder, and S. Phansee, "Evaluation of CFD to Determine Two-Dimensional Airfoil Characteristics for Rotorcraft Applications." *Journal of the American Helicopter Society*, 2006. **Vol. 51**(1): p. 70-79.
  3. Smith, M.J., B. Koukol, T.R. Quackenbush, and D.A. Wachspress. "Reverse- and Cross-Flow Aerodynamics for High-Advance-Ratio Flight." *35th European Rotorcraft Forum*. 2009. Hamburg, Germany.
  4. Bagai, A. and J.G. Leishman, "Rotor Free-Wake Modeling Using a Relaxation Technique - Including Comparisons with Experimental Data." *Journal of the American Helicopter Society*, 1995. **40**(3): p. pp.29-41.
  5. Bhagwat, M.J. and J.G. Leishman, "Rotor Aerodynamics During Maneuvering Flight Using a Time-Accurate Free-Vortex Wake." *Journal of the American Helicopter Society*, 2003. **48**(3): p. 143-158.
  6. Johnson, W. "Technology Drivers in the Development of CAMRAD II." *NASA/AHS Aeromechanics Specialists Conference*. 1994. San Francisco.
  7. Johnson, W. "Rotorcraft Aerodynamics Models for Comprehensive Analysis." *54th Annual Forum of the American Helicopter Society*. 1998. Washington, D.C.
  8. Quackenbush, T.R. and D.B. Bliss, "Free Wake Flow Field Calculations for Rotorcraft Interactional Dynamics." *Vertica*, 1990. **14**(3): p. 313-327.
  9. Quackenbush, T.R., D.B. Bliss, and D.A. Wachspress, "New Free-Wake Analysis of Rotorcraft Hover Performance Using Influence Coefficients." *Journal of Aircraft*, 1989. **26**(12): p. pp.1090-1097.
  10. Wachspress, D.A., T.R. Quackenbush, and A.H. Boschitsch. "First-Principles, Free-Vortex Wake Model for Helicopters and Tiltrotors." *59th Annual Forum of the American Helicopter Society*. 2003. Phoenix, AZ.
  11. Wachspress, D.A., T.R. Quackenbush, and A.H. Boschitsch, "Rotorcraft Interactional Aerodynamics with Fast Vortex/Fast Panel Methods." *Journal of the American Helicopter Society*, 2003. **Vol. 48**(No. 4).
  12. Holst, T.L. and T.H. Pulliam. "Optimization of Overset Solution Adaptive Grids for Hovering Rotorcraft Flows." *AHS Aeromechanics Specialist's Conference*. 2010. San Francisco, CA.
  13. Usta, E., "Application of a Symmetric Total Variation Diminishing Scheme to Aerodynamics of Rotors." 2002, Georgia Institute of Technology.
  14. Usta, E. and L.N. Sankar. "Application of High Order Schemes to Aerodynamics of Hovering Rotors." *AHS Aerodynamics, Acoustics, and Test and Evaluation Technical Specialists Meeting*. 2002. San Francisco, CA.
  15. Usta, E., B.E. Wake, T.A. Egolf, and L.N. Sankar. "Application of Symmetric Total Variation Diminishing Scheme to Aerodynamics and Aeroacoustics of Rotors." *57th Annual Forum of the American Helicopter Society*. 2001. Washington, D.C.
  16. Kim, H., M.H. Williams, and A.S. Lyrintzis, "Improved Method for Rotor Wake Capturing." *Journal of Aircraft*, 2002. **Vol.39**(No. 5): p. pp. 794-803.
  17. van der Ven, H. and O.J. Boelens. "Towards Affordable CFD Simulations of Rotors in Forward Flight - A Feasibility Study with Future Applications to Vibrational Analysis." *American Helicopter Society 59th Annual Forum*. 2003. Phoenix, AZ.
  18. Duque, E.P.N., L.N. Sankar, S. Menon, O. Bachau, S. Ruffin, M. Smith, K. Ahuja, K.S. Brentner, L.N. Long, P.J. Morris, and F. Gandhi. "Revolutionary Physics-Based Design Tools for Quiet Helicopters." *44th AIAA Aerospace Sciences Meeting and Exhibit*. 2006. Reno, NV: AIAA-2006-1068.
  19. Potsdam, M.A. and R.C. Strawn, "CFD Simulations of Tiltrotor Configurations in Hover." *Journal of the American Helicopter Society*, 2005. **Vol. 50**(No. 1): p. pp. 82-94.
  20. Strawn, R.C. and M.J. Djomenhri, "Computational Modeling of Hovering Rotor and Wake Aerodynamics." *Journal of Aircraft*, 2002. **Vol. 39**(No. 5): p. pp. 786-793.
  21. Costes, M. "Analysis of the VC2 Vorticity Confinement Scheme." *62nd Annual Forum of the American Helicopter Society*. 2006. Phoenix, AZ.
  22. Dietz, W., M. Fan, J. Steinhoff, and Y. Wenren. "Application of Vorticity Confinement to Prediction of the Flow over Complex Bodies: A Survey of Recent Results." *AIAA CFD Conference*. 2001. Anaheim, CA.
  23. Steinhoff, J., Y. Wenren, and F.X. Caradonna. "Application of Vorticity Confinement to Rotorcraft Flows." *31st European Rotorcraft Forum*. 2005. Firenze, Italy.



24. Wang, C.M., J.O. Bridgeman, J.S. Steinhoff, and W. Yonghu. "The Application of Computational Vorticity Confinement to Helicopter Rotor and Body Flows." *49th Annual Forum of the American Helicopter Society*. 1993. St. Louis, Missouri.
25. Wenren, Y., M. Fan, L. Wang, M. Xiao, and J. Steinhoff. "Application of Vorticity Confinement to Prediction of the Flow over Complex Bodies." *AIAA Journal*, 2003. **Vol. 41(5)**: p. 809-816.
26. Bhagwat, M.J., M.A. Moulton, and F.X. Caradonna. "Development of a CFD-Based Hover Performance Prediction Tool for Engineering Analysis." *American Helicopter Society 61st Annual Forum*. 2005. Grapevine, TX.
27. Hariharan, N. and L.N. Sankar. "A Review of Computational Techniques for Rotor Wake Modeling." *38th Aerospace Sciences Meeting & Exhibit*. 2000. Reno, Nevada.
28. Khanna, H. and J.D. Baeder. "Coupled Free-Wake/CFD Solutions for Rotors in Hover Using a Field Velocity Approach." *52nd Annual Forum of the American Helicopter Society*. 1996. Washington, D.C.
29. Moulton, M.A., J.O. Bridgeman, and F.X. Caradonna. "Development of an Overset/Hybrid CFD Method for the Prediction of Hovering Performance." *53 Annual Forum of the American Helicopter Society*. 1997. Virginia Beach, VA.
30. Moulton, M.A., Y. Wenren, and F.X. Caradonna. "Free-Wake Hover Flow Prediction with a Hybrid Potential/Navier-Stokes Solver." *AHS 55th Annual Forum*. 1999. Montreal, Canada: American Helicopter Society.
31. Roberts, T.W. and E.M. Murman. "A Computational Method for Helicopter Vortex Wakes." *AIAA 17th Fluid Dynamics, Plasma Dynamics, & Lasers Conf*. 1984. Snowmass, CO.
32. Roberts, T.W. and E.M. Murman. "Solution Method for a Hovering Helicopter Rotor Using the Euler Equations." *AIAA 23rd Aerospace Sciences Meeting*. 1985. Reno, NV.
33. Egolf, T.A., N. Rajmohan, E. Reed, and L.N. Sankar. "A Hybrid CFD Method for Coaxial Rotor Performance Prediction in Forward Flight." *AHS Specialist's Conference on Aeromechanics*. 2010. San Francisco, CA.
34. Rajmohan, N., L.N. Sankar, O. Bachau, B. Charles, S.M. Makinen, and T.A. Egolf. "Application of Hybrid Methodology to Rotors in Steady and Maneuvering Flight." *64th Annual Forum of the American Helicopter Society*. 2008. Montreal, Canada.
35. Thomas, S., S. Ananthan, and J.D. Baeder. "Wake-Coupling CFD-CSD Analysis of Helicopter Rotors in Steady and Maneuvering Flight Conditions." *AHS Specialist's Conference on Aeromechanics*. 2010. San Francisco, CA.
36. Bhagwat, M.J., M. Moulton, and F.X. Caradonna. "Recent Advances in the Embedded-Wake Approach to Hover Performance Prediction." *AHS 4th Decennial Specialist's Conference on Aeromechanics*. 2004. San Francisco, CA.
37. Datta, A., J. Sitaraman, J.D. Baeder, and I. Chopra. "Analysis Refinements for Prediction of Rotor Vibratory Loads in High-Speed Forward Flight." *American Helicopter Society 60th Annual Forum*. 2004. Baltimore, MD.
38. Datta, A., J. Sitaraman, I. Chopra, and J.D. Baeder. "Improved Comprehensive Analysis for Prediction of Rotor Vibratory Loads in High-Speed Forward Flight." *American Helicopter Society 60th Annual Forum*. 2004. Baltimore, MD.
39. Berkman, M.E., L.N. Sankar, C.R. Berezin, and M.S. Torok. "A Navier-Stokes/Full Potential/Free Wake Method for Advancing Multi-Bladed Rotors." *53rd American Helicopter Society Annual Forum*. 1997. Virginia Beach, VA.
40. Anusonti-Inthra, P. "Development of Rotorcraft Wake Capturing Methodology Using Fully Coupled CFD and Particle Vortex Transport Method." *62nd Annual Forum of the American Helicopter Society*. 2006. Phoenix, AZ.
41. Anusonti-Inthra, P. and M. Floros. "Coupled CFD and Particle Vortex Transport Method: Wing Performance and Wake Validations " *38th AIAA Fluid Dynamics Conference and Exhibit*. 2008. Seattle, WA: AIAA-2008-4177
42. Cottet, G.-H. and P.D. Koumoutsakos, *Vortex Methods: Theory and Practice*. 2000, Cambridge, UK: Cambridge University Press. pp.313.
43. He, C. and J. Zhao, "Modeling Rotor Wake Dynamics with Viscous Vortex Particle Method." *AIAA Journal*, 2009. **Vol. 47(No. 4)**: p. pp. 902-915.
44. Zhao, J. and C. He, "A Viscous Vortex Particle Model for Rotor Wake and Interference Analysis." *Journal of the American Helicopter Society*, 2010. **Vol. 55(No. 1)**.
45. Brown, R.E., "Rotor Wake Modeling for Flight Dynamic Simulation of Helicopters." *AIAA Journal*, 2000. **Vol. 38(No. 1)**: p. 57-63.

46. Brown, R.E. and A.J. Line, "Efficient High-Resolution Wake Modeling Using the Vorticity Transport Equation." *AIAA Journal*, 2005. **Vol. 43**(No. 7): p. 1434-1443.
47. Brown, R.E. and G.R. Whitehouse, "Modelling Rotor Wakes in Ground Effect." *Journal of the American Helicopter Society*, 2004. **Vol. 49**(No. 3): p. 238-249.
48. Whitehouse, G.R., A.H. Boschitsch, T.R. Quackenbush, D.A. Wachspress, and R.E. Brown. "Novel Eulerian Vorticity Transport Wake Module for Rotorcraft Flow Analysis." *8th Symposium on Overset Composite Grids & Solution Technology*. 2006. Houston, TX.
49. Whitehouse, G.R., A.H. Boschitsch, T.R. Quackenbush, D.A. Wachspress, and R.E. Brown. "Novel Eulerian Vorticity Transport Wake Module for Rotorcraft Flow Analysis." *63rd Annual Forum of the American Helicopter Society*. 2007. Virginia Beach, VA.
50. Whitehouse, G.R. and H. Tadghighi. "Investigation of Hybrid Grid-Based CFD Methods for Rotorcraft Flow Analysis." *AHS Specialist's Conference on Aeromechanics*. 2010. San Francisco, CA.
51. Schumann, U. and R.A. Sweet, "A Direct Method for the Solution of Poisson's Equation with Neumann Boundary Conditions on a Staggered Grid of Arbitrary Size." *Journal of Computational Physics*, 1976. **Vol. 20**(No. 2): p. pp. 171-182.
52. Whitehouse, G.R. and R.E. Brown, "Modelling the Mutual Distortions of Interacting Helicopter and Aircraft Wakes." *Journal of Aircraft*, 2003. **Vol. 40**(No. 3): p. pp. 440-449.
53. Line, A.J., "Computational Modelling of Helicopter High-Frequency Dynamics." 2005, PhD Thesis, Department of Aeronautics Imperial College London.
54. Line, A.J. and R.E. Brown. "Efficient High-Resolution Wake Modelling using the Vorticity Transport Equation." *60th Annual Forum of the American Helicopter Society*. 2004. Baltimore, MD.
55. Toro, E.F. "A Weighted Average Flux Method for Hyperbolic Conservation Laws." *Royal Society of London, Series A: Mathematical and Physical Sciences*,. 1989.
56. Brown, R.E., "Rotor Wake Modeling for Flight Dynamic Simulation of Helicopters." *AIAA Journal*, 2000. **Vol. 38**(1): p. 57-63.
57. Harris, R.E., E.F. Sheta, and S.D. Habchi. "An Efficient Adaptive Cartesian Vorticity Transport Solver for Rotorcraft Flowfield Analysis." *48th AIAA Aerospace Sciences Meeting*. 2010. Orlando, FL: AIAA-2010-1072.
58. Boschitsch, A.H. and T.R. Quackenbush. "Adaptive Grid Computation of Transonic Flows Through Cascades and Investigation of Chordwise Bending Upon Aeroelastic Response." *32nd AIAA Aerospace Sciences Meeting & Exhibit*. 1994. Reno, NV.: AIAA-1994-0145.
59. Boschitsch, A.H. and T.R. Quackenbush, "High Accuracy Fluid-Structure Interaction in Transonic Cascades," *31st AIAA Aerospace Sciences Meeting*. 1993, AIAA-1993-0485: Reno, NV.
60. Boschitsch, A.H. and T.R. Quackenbush. "Prediction of Rotor Aeroelastic Response Using a New Coupling Scheme." *Fifth Workshop on Dynamics and Aeroelastic Stability Modeling of Rotorcraft Systems*. 1993. Rensselaer Polytechnic Institute, Troy, NY.
61. Boschitsch, A.H. and T.R. Quackenbush. "Prediction of Rotor Aeroelastic Response Using a New Coupling Scheme." *25th AIAA Fluid Dynamics Conference*. 1994. Colorado Springs, CO.: AIAA-1994-2269.
62. Keller, J.D., G.R. Whitehouse, A.H. Boschitsch, J. Nadal, J. Jeffords, and M. Quire. "Computational Fluid Dynamics for Flight Simulator Ship Airwake Modeling." *Interservice/Industry Training, Simulation, and Education Conference (IITSEC) 2007*. 2007. Orlando, FL.
63. Buning, P. "Consolidation of Time-Accurate, Moving Body Capabilities in OVERFLOW " *6th Overset Composite Grid and Solution Technology Symposium*. 2002. Fort Walton Beach, FL.
64. Slotnick, J.P., P.G. Buning, and R.H. Nichols. "OVERFLOW Flow Solver Overview." *8th Symposium on Overset Composite Grids & Solution Technology*. 2006. Houston, TX.
65. Chan, W.M., R.J. Gomez, S.E. Rogers, and P.G. Buning. "Best Practices in Overset Grid Generation." *32nd AIAA Fluid Dynamics Conference*. 2002. St. Louis, MO: AIAA-2002-3191.
66. Anderson, W.K. and D.L. Bonhaus, "An Implicit Upwind Algorithm for Computing Turbulent Flows on Unstructured Grids." *Computers in Fluids*, 1994. **Vol. 23**(No. 1): p. 1-21.
67. Nielsen, E.J. and W.K. Anderson, "Improvements in Aerodynamic Design Optimization on Unstructured Meshes." *AIAA Journal*, 2002. **Vol. 40**, (No. 6): p. pp. 1155-1163.

68. Biedron, R.T. and E.M. Lee-Rausch. "Rotor Airloads Prediction Using Unstructured Meshes and Loose CFD/CSD Coupling." *26th AIAA Applied Aerodynamics Conference*. 2008. Honolulu, HI: AIAA-2008-7341.
69. Chorin, A.J., "The Numerical Solution of the Navier-Stokes Equations for an Incompressible Fluid " Bull. Amer. Math. Soc., 1967. **Vol. 73**: p. pp. 928-931.
70. O'Brien, D.M., "Analysis Of Computational Modeling Techniques For Complete Rotorcraft Configurations," *School of Aerospace Engineering*. 2006, Georgia Institute of Technology, PhD.
71. Rajmohan, N., J. Bain, M. Nucci, L.N. Sankar, R. Flemming, T.A. Egolf, and R. Kreeger. "Icing Studies for the UH-60A Rotor in Forward Flight." *AHS Specialist's Conference on Aeromechanics*. 2010. San Francisco, CA.
72. Caradonna, F.X., "Developments and Challenges in Rotorcraft Aerodynamics." 2000.
73. Ramachandran, K., S. Schlechtriem, F.X. Caradonna, and J. Steinhoff. "The Application of Vorticity Embedding to the Computation of Advancing Rotor Flows." *AHS 49th Annual Forum*. 1993. St. Louis, Missouri: American Helicopter Society, Inc.
74. Tung, C., F.X. Caradonna, and W.R. Johnson, "The Prediction of Transonic Flows on an Advancing Rotor." *Journal of the American Helicopter Society*, 1986. **31**(3).
75. Strawn, R.C., F.X. Caradonna, and E.P.N. Duque, "0 Years of Rotorcraft Computational Fluid Dynamics Research and Development." *Journal of the American Helicopter Society*, 2006. **Vol. 51**(No. 1): p. pp.5-21.
76. Sitaraman, J., V.S. Iyengar, and J.D. Baeder. "On the Field Velocity Approach and Geometric Conservation Law for Unsteady Flow Simulations." *AIAA Applied CFD Conference*. 2003. Orlando, FL.
77. Sitaraman, J. and J.D. Baeder. "On Field velocity approach and Geometric Conservation Law for Unsteady Flow Simulations." *16th AIAA Computational Fluid Dynamics Conference*. 2003. Orlando, FL: AIAA-2003-3835
78. Glauert, H., *The Elements of Aerofoil and Airscrew Theory*. 2nd ed. 1948: Cambridge University Press.
79. Drela, M. "XFOIL: An Analysis and Design System for Low Reynolds Number Airfoils,." *Conference on Low Reynolds Number Airfoil Aerodynamics*. 1989. University of Notre Dame, IN.
80. Hoerner, S.F., *Fluid-Dynamic Drag*. 1965, New York, NY: Hoerner Fluid Dynamics.
81. Fulton, M.V. "Aeromechanics of the Active Elevon Rotor." *61st Annual Forum of the American Helicopter Society*. 2005. Grapevine, TX.
82. Kempka, S.N., J.H. Strickland, M.W. Glass, J.S. Peery, and M.S. Ingber, "Velocity Boundary Conditions for Vorticity Formulations of the Incompressible Navier-Stokes Equations." 1995, Sandia National Laboratories, SAND94-1735: Albuquerque, NM.
83. Caradonna, F.X. and C. Tung, "Experimental and Analytical Studies of a Model Helicopter Rotor in Hover." 1981, NASA-TM-81232, USAAVRADCOR TR-81-A-23.
84. Lynch, E. and M.J. Smith. "Hybrid RANS-LES Turbulence Models on Unstructured Grids " *38th AIAA Fluid Dynamics Conference and Exhibit*. 2008. Seattle, WA: AIAA-2008-3854